Title
Protective responses to sublytic complement in the retinal pigment epithelium

Journal
Proceedings of the National Academy of Sciences of the United States of America, 113(31)

ISSN
0027-8424

Authors
Tan, Li Xuan
Toops, Kimberly A
Lakkaraju, Aparna

Publication Date
2016-08-02

DOI
10.1073/pnas.1523061113

Peer reviewed

Protective responses to sublytic complement in the retinal pigment epithelium

Li Xuan Tan[a,b], Kimberly A. Toops[a,c], and Aparna Lakkaraju[a,b,c,1]

[a]Department of Ophthalmology and Visual Sciences, School of Medicine and Public Health, University of Wisconsin, Madison, WI 53706; [b]Division of Pharmaceutical Sciences, School of Pharmacy, University of Wisconsin, Madison, WI 53706; and [c]McPherson Eye Research Institute, University of Wisconsin, Madison, WI 53706

Edited by Catherine Bowes Rickman, Duke University Medical Center, Durham, NC, and accepted by Editorial Board Member Jeremy Nathans June 13, 2016 (received for review November 23, 2015)

The retinal pigment epithelium (RPE) is a key site of injury in inherited and age-related macular degenerations. Abnormal activation of the complement system is a feature of these blinding diseases, yet how the RPE combats complement attack is poorly understood. The complement cascade terminates in the cell-surface assembly of membrane attack complexes (MACs), which promote inflammation by causing aberrant signal transduction. Here, we investigated mechanisms crucial for limiting MAC assembly and preserving cellular integrity in the RPE and asked how these are compromised in models of macular degeneration. Using polarized primary RPE and the pigmented *Abca4*$^{-/-}$ Stargardt disease mouse model, we provide evidence for two protective responses occurring within minutes of complement attack, which are essential for maintaining mitochondrial health in the RPE. First, accelerated recycling of the membrane-bound complement regulator CD59 to the RPE cell surface inhibits MAC formation. Second, fusion of lysosomes with the RPE plasma membrane immediately after complement attack limits sustained elevations in intracellular calcium and prevents mitochondrial injury. Cholesterol accumulation in the RPE, induced by vitamin A dimers or oxidized LDL, inhibits these defense mechanisms by activating acid sphingomyelinase (ASMase), which increases tubulin acetylation and derails organelle traffic. Defective CD59 recycling and lysosome exocytosis after complement attack lead to mitochondrial fragmentation and oxidative stress in the RPE. Drugs that stimulate cholesterol efflux or inhibit ASMase restore both these critical safeguards in the RPE and avert complement-induced mitochondrial injury in vitro and in *Abca4*$^{-/-}$ mice, indicating that they could be effective therapeutic approaches for macular degenerations.

macular degeneration | inflammation | cholesterol | mitochondria | drug targets

The complement system is an important regulator of immunity and inflammation. Complement activation by the classical, alternative, or lectin pathways results in the assembly of C5b-9 membrane attack complexes (MACs), which form membrane pores and cause target cell lysis. Within the eye, a low level of constant complement activity is necessary for immune surveillance, and several membrane-bound and soluble regulators prevent excessive complement activation (1). An imbalance between complement activation and inhibition in the retina is implicated in the pathogenesis of age-related macular degeneration (AMD), which causes central vision loss in more than 30 million people globally (reviewed in refs. 2–4).

Evidence suggests that the retinal pigment epithelium (RPE), which helps maintain ocular immune privilege, is the first line of defense against unregulated complement activation in the retina (5). The complement cascade is activated by insults that disturb RPE homeostasis, including defective clearance of phagocytosed photoreceptor outer segments (6) and abnormal accumulation of vitamin A dimers (7–9) or oxidized lipids (10) in the RPE. Studies also show that exposure to sublytic levels of MAC alters RPE barrier integrity, causes mitochondrial stress, and induces secretion of VEGF and proinflammatory cytokines (11, 12). Thus, RPE dysfunction activates the complement cascade, which can promote further RPE damage and establish a vicious cycle of chronic inflammation within the retina (13).

How the RPE counters MAC formation and eliminates MAC pores to preserve cell integrity is not well understood (14). The alternative pathway of complement activation begins with the spontaneous hydrolysis of C3 and sequential recruitment of C5b, C6, C7, C8, and finally C9, which polymerizes to form the MAC (2). The membrane-bound complement regulator CD59, which binds C8 and C9, prevents recruitment of C9 to the C5b-8 complex and thus inhibits the final step of MAC assembly (15). Immunostaining of human donor tissue shows that CD59 is predominantly found on the apical surface (16). Decreased CD59 expression (16) and increased MAC deposition in sub-RPE drusen and at the RPE-choroid interface (13, 17) have been detected in AMD patient tissues, pointing to a breakdown in mechanisms that prevent MAC assembly. Activated complement components have also been detected in retinal tissue from the *Abca4*$^{-/-}$ mouse model of Stargardt macular dystrophy, characterized by lipofuscin accumulation and accelerated formation of vitamin A dimers, such as A2E, in the RPE (7, 8). There appears to be a direct correlation between levels of vitamin A dimers in the RPE and complement activation, because inhibiting vitamin A dimerization decreases both A2E levels and complement activity in *Abca4*$^{-/-}$ mice (7). How the accumulation of vitamin A dimers leads to complement activation in Stargardt disease remains unclear.

If MACs and other complement proteins are predominantly found in the sub-RPE region in macular dystrophies, what is the role of CD59 on the apical surface of the RPE? Recent studies suggest that complement activation in the subretinal space also plays a role in AMD: Oxidative modifications of photoreceptor lipids such

Significance

The complement system regulates immune defense and inflammation. Abnormal complement activation in the retina is associated with blinding macular degenerations, which have limited treatment options. The retinal pigment epithelium (RPE) is an initial site of injury in macular degenerations, but mechanisms that protect the RPE from complement-mediated damage are unclear. Here, we identify two critical responses to complement in the RPE: accelerated recycling of the complement inhibitor CD59 and lysosome-mediated membrane repair. We show that in models of macular degeneration, excess cholesterol impairs both defense mechanisms, resulting in mitochondrial damage. Drugs that decrease RPE cholesterol restore these mechanisms and help the RPE combat complement attack. Our studies identify promising drug targets to preserve RPE health and function in macular degenerations.

Author contributions: L.X.T., K.A.T., and A.L. designed research, performed research, analyzed data, and wrote the paper.

Conflict of interest statement: L.X.T., K.A.T., and A.L. are listed on a patent application filed by the Wisconsin Alumni Research Foundation at the University of Wisconsin–Madison on the use of acid sphingomyelinase inhibitors to treat macular degenerations. This patent has not yet been issued.

This article is a PNAS Direct Submission. C.B.R. is a guest editor invited by the Editorial Board.

[1]To whom correspondence should be addressed. Email: lakkaraju@wisc.edu.

This article contains supporting information online at www.pnas.org/lookup/suppl/doi:10.1073/pnas.1523061113/-/DCSupplemental.

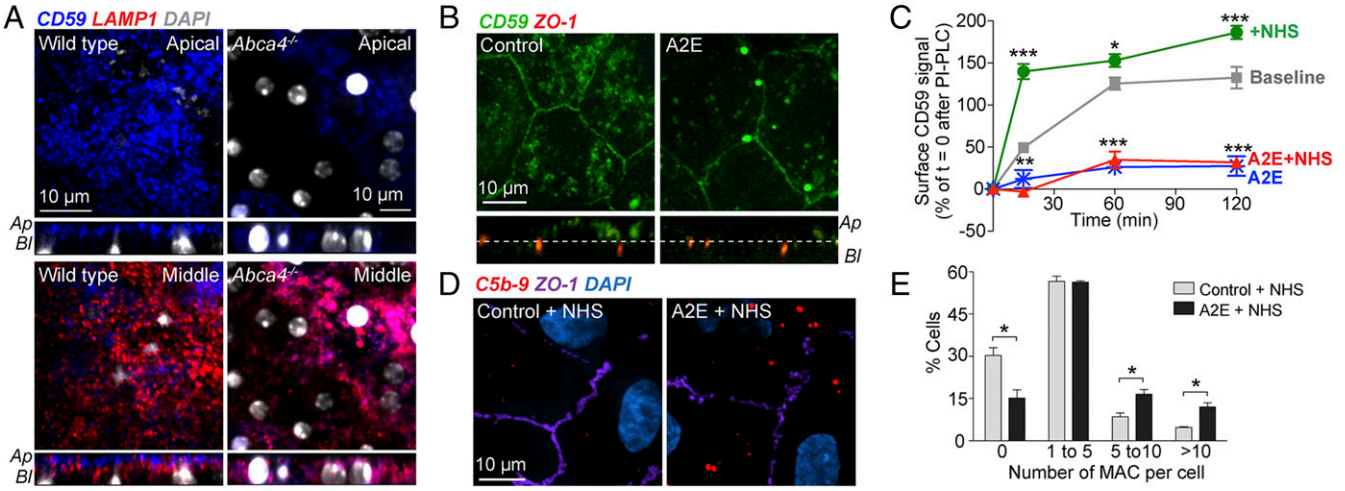

Fig. 1. CD59 recycling and MAC deposition after complement attack. (*A*) Single-plane *en face* and *x-z* images of CD59 immunostaining (blue) in mouse RPE flatmounts. Apical and middle slices are shown. LAMP1 (red) labels lysosomes. (*B*) Immunofluorescence images of surface CD59 (green) in polarized primary RPE ± A2E. In the *x-z* images, ZO-1 (red) demarcates apical (Ap) and basolateral (Bl) cell membranes. (*C*) Recovery of surface CD59 fluorescence after PI-PLC treatment in control RPE (Baseline, gray squares), after complement (NHS, green circles), and cells with A2E alone (blue asterisks) or exposed to complement (A2E + NHS, red triangles). Mean ± SEM, $n \geq 60$ cells per condition. $^*P < 0.05$; $^{**}P < 0.001$, and $^{***}P < 0.0001$ relative to baseline values. (*D*) MAC immunostaining (red) on the RPE surface after 10% NHS for 10 min. ZO-1 is in purple. (*E*) Quantification of MAC deposition. $^*P < 0.05$, mean ± SEM, $n \geq 150$ cells per condition.

as malondialdehyde activate complement (18); subretinal drusen from AMD patients have complement components (16); and retinal detachment down-regulates CD59, leading to MAC deposition in the photoreceptor-RPE region (19).

Here, using polarized primary RPE monolayers and *Abca4*$^{-/-}$ mice, we demonstrate that accelerated recycling of CD59 to the apical surface of the RPE following complement attack is a critical rapid response that helps combat complement-mediated injury. A second rapid response is the fusion of RPE lysosomes with the plasma membrane within seconds of complement attack to preserve cell integrity. Our data show that cholesterol accumulation, due to vitamin A dimers in *Abca4*$^{-/-}$ mice RPE (20, 21) or oxidized LDL (10), interferes with both these protective mechanisms. Defective CD59 recycling and lysosome exocytosis allow MAC pores to persist, culminating in mitochondrial damage and oxidative stress. Cholesterol-mediated activation of acid sphingomyelinase (ASMase) (20), which sabotages microtubule-mediated organelle traffic, interferes with CD59 transport to the cell surface and lysosome-plasma membrane fusion. In agreement with this, drugs that decrease RPE cholesterol or inhibit ASMase restore both protective responses and limit complement-induced mitochondrial injury in vitro and in *Abca4*$^{-/-}$ mice. These data identify cholesterol and ASMase as therapeutic targets for preventing RPE dysfunction in Stargardt disease and other retinal dystrophies associated with lipofuscin accumulation.

Results

Recycling of CD59 and MAC Deposition in the RPE. Analysis of RPE flatmounts and retinal cryosections showed that in wild-type mice, CD59 was predominantly on the apical membrane of the RPE (Fig. 1*A* and Fig. S1 *A* and *B*). In *Abca4*$^{-/-}$ RPE, CD59 was mainly intracellular and colocalized with the lysosomal membrane protein (LAMP) 1 (Fig. 1*A*). Similar results were observed in polarized primary porcine RPE monolayers: significantly less CD59 was present on the apical surface of cells treated with the vitamin A dimer A2E (10 μM for 6 h, followed by incubation in fresh culture medium for 48 h; ref. 20) compared with control cells (Fig. 1*B* and Fig. S1*I*). These data suggest that vitamin A dimers prevent CD59 trafficking in polarized primary RPE and in *Abca4*$^{-/-}$ RPE.

CD59 is a glycosylphosphatidylinositol-anchored protein (GPI-AP) that undergoes cholesterol-dependent internalization and recycling to the cell surface. Cholesterol depletion accelerates GPI-AP recycling, whereas cholesterol overload reroutes GPI-APs to lysosomes (22). Because vitamin A dimers cause cholesterol accumulation in the RPE (20, 21), they could potentially interfere with CD59 trafficking. To follow CD59 recycling, we treated RPE monolayers with phosphatidylinositol-specific phospholipase C (PI-PLC), which removes cell surface GPI-APs such as CD59 (23). Cell surface CD59 was completely restored ~60 min after

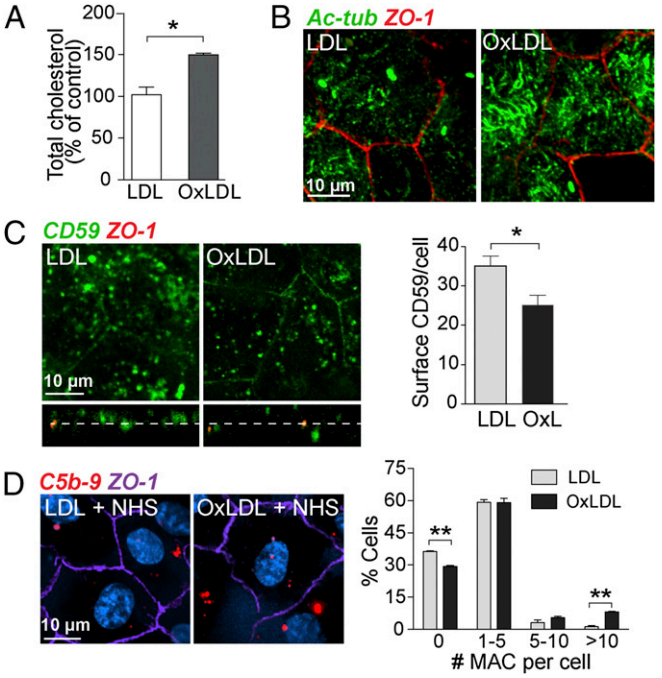

Fig. 2. Excess RPE cholesterol increases susceptibility to complement. (*A*) Total cholesterol in polarized primary RPE treated with LDL or OxLDL. Mean ± SEM, $n = 4$ independent experiments. $^*P < 0.01$. Immunostaining of acetylated tubulin (*B*) and CD59 (*C*), both green, in RPE treated with LDL or OxLDL. ZO-1 is in red. For quantification in *C*, mean ± SEM, ≥ 120 cells per condition. $^*P < 0.01$. (*D*) MAC immunostaining and quantification (red) on the RPE surface after exposure to 10% NHS for 10 min. ZO-1 is in purple. Mean ± SEM, $n \geq 150$ cells per condition. $^{**}P < 0.001$.

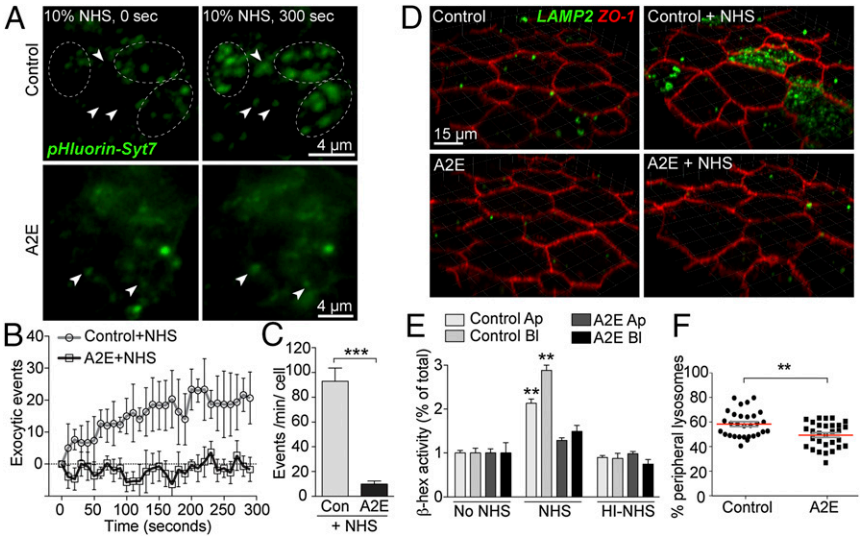

Fig. 3. Exposure to complement stimulates lysosome exocytosis. (*A*) Stills from TIRF imaging of pHluorin-Syt7 (green) in RPE exposed to 10% NHS. Images shown were captured immediately after NHS was added ($t = 0$ s) and 300 s later. See Movie S1 (control cells) and Movie S2 (cells with A2E). Arrowheads and dashed ellipses denote areas with increased pHluorin signal indicating lysosome fusion. Cumulative number of events (*B*) and event frequency in control RPE and RPE with A2E (*C*). Mean ± SEM, $***P < 0.0001$. (*D*) Surface LAMP2 immunolabeling (green) after 10% NHS for 10 min. ZO-1 is in red. (*E*) β-Hex activity in apical and basal media from cells exposed to 10% NHS or heat-inactivated NHS (HI-NHS). Mean ± SEM, $n = 5$. $**P < 0.001$ relative to all other conditions, one-way ANOVA with Bonferroni's post hoc test. (*F*) Number of lysosomes within 500 nm of the plasma membrane in primary RPE, $n = 30$ cells per group. $**P < 0.005$.

treatment with PI-PLC in control RPE monolayers. In contrast, in cells with A2E, surface CD59 levels remained significantly less than controls even after 120 min (Fig. 1*C*).

Structural studies show that C5b-8 on the membrane induces conformational changes in CD59 that enable the latter to bind to C9 and inhibit MAC formation (15). Thus, only CD59 on the cell surface can respond to C5b-8, suggesting that sublytic complement attack could modulate CD59 recycling. To test this theory, we exposed RPE monolayers for 10 min to either 10% normal human serum (NHS) or 60 μg/mL purified C9 protein (mean physiological C9 concentration) (11) reconstituted in 10% C9-depleted serum. Analysis of lactate dehydrogenase (LDH) activity in the apical and basolateral media confirmed that both treatments were sublytic, i.e., caused <5% cytotoxicity (24) (Fig. S1 *C* and *D*). Exposure to NHS (Fig. 1*C*) or C9 (Fig. S1*E*) caused an ~threefold increase in CD59 recycling within 15 min after PI-PLC treatment, compared with baseline recovery in untreated cells (Fig. 1*C*) or cells exposed to C9-depleted serum alone (Fig. S1*E*). This accelerated CD59 recycling in response to complement was not observed in cells with A2E (Fig. 1*C*). Acute treatment with A2E, as in the CD59 recycling experiments, did not alter CD59 protein levels (Fig. S1*F*); however, CD59 protein was significantly reduced after chronic treatment with A2E (50 nM for 3 wk) (Fig. S1*F*) and in 6-mo-old *Abca4*$^{-/-}$ mice RPE (Fig. S1*G*; antibody validated in Fig. S2). Because *CD59* gene expression is not altered in pigmented *Abca4*$^{-/-}$ mice RPE (7), the data in Fig. 1*A* and Fig. S1 *F* and *G* suggest that A2E-induced cholesterol storage shunts CD59 toward lysosomal degradation, resulting in decreased CD59 protein levels over time.

Exposure of RPE to either NHS or C9 caused MAC deposition, which was significantly increased in cells with A2E (Fig. 1 *D* and *E* and Fig. S1*H*), likely due to less cell surface CD59. We have shown that excess cholesterol in RPE with vitamin A dimers activates ASMase, which interferes with organelle traffic by acetylating microtubules (MT) (20). To investigate how excess cholesterol and MT acetylation impacts CD59 trafficking, we treated RPE monolayers with either U18666A to increase cholesterol (25) and, thereby, acetylated MT (20), or with the HDAC6 inhibitor tubacin, which prevents MT deacetylation (26). Similar to A2E, both drugs decreased cell surface CD59 and increased MAC deposition after complement exposure (Fig. S1*I*). Thus, cholesterol-induced MT acetylation in RPE with vitamin A dimers prevents rapid CD59 recycling in response to complement and enables MAC assembly on the cell surface.

RPE Cholesterol Modulates Susceptibility to Sublytic MACs. To confirm that excess cholesterol promotes MAC deposition after complement attack, we used oxidized LDL (OxLDL) to increase RPE cholesterol independent of vitamin A dimers (Fig. 2*A*). OxLDL also increased acetylated tubulin (Fig. 2*B*) and decreased cell surface CD59 (Fig. 2*C*). Complement attack resulted in more MAC deposition in OxLDL-treated cells, compared with RPE treated with LDL (Fig. 2*D*). Because vitamin A dimers, oxidized lipids, and lipoproteins are all implicated in the pathogenesis of macular dystrophies (8, 10, 18), our data point to excess cholesterol as a common etiological factor that could link these insults with abnormal complement activation in the outer retina.

Sublytic Complement Attack Induces Rapid Lysosome Exocytosis. One of the earliest detectable events after complement exposure is an increase in intracellular calcium ($[Ca^{2+}]_i$) via influx through MAC pores (24) and/or activation of endogenous ion channels (27). In many cell types, elevated $[Ca^{2+}]_i$ has been shown to trigger fusion of lysosomes with the plasma membrane (25, 28). Lysosome exocytosis, mediated by the lysosomal calcium sensor synaptotagmin 7 (Syt7), is vital for preserving membrane integrity after exposure to pore-forming toxins (29). We used live-cell imaging by total internal reflection fluorescence (TIRF) microscopy and complementary biochemical assays to determine whether sublytic MACs stimulate lysosome exocytosis in the RPE. We transfected primary RPE with Syt7 tagged with pHluorin, whose fluorescence is quenched in acidic lysosomal pH and relieved upon exposure to neutral pH after exocytosis (30). Individual exocytic events after addition of 10% NHS were detected as bright flashes of unquenched pHluorin in control cells (Fig. 3*A* and Movie S1). Cells with A2E had significantly fewer detectable exocytic events (Fig. 3 *A* and *B* and Movie S2): an average of 9 events per min compared with 93 events per min in control cells (Fig. 3*C*).

Lysosome exocytosis causes transient appearance of lysosomal membrane proteins (e.g., LAMP2) on the plasma membrane and release of lysosomal hydrolases such as β-hexosaminidase (β-hex) into the extracellular medium (25). We detected LAMP2 on the RPE cell surface after a 10-min exposure to either 10% NHS (Fig. 3*D*) or 60 μg/mL C9 (Fig. S3*A*). Live-cell TIRF imaging showed that lysosome–plasma membrane interactions are transient with both full and partial kiss-and-run fusions; therefore, we were able to detect LAMP2 mostly on the apical surface of a subset of cells. β-hex activity was detected in both the apical and basolateral media after complement attack in control cells, suggesting that lysosomes fuse with both domains of the RPE (Fig. 3*E*). No β-hex activity was detected after exposure to heat-inactivated NHS; thus, only active complement components stimulate lysosome exocytosis. Consistent with TIRF imaging, RPE cells with A2E had significantly less surface LAMP2 and β-hex activity in the medium after complement attack (Fig. 3 *D* and *E*).

TIRF imaging showed that lysosomes exocytose within seconds of complement exposure, indicating that a pool of lysosomes predocked at the plasma membrane are rapidly mobilized in response

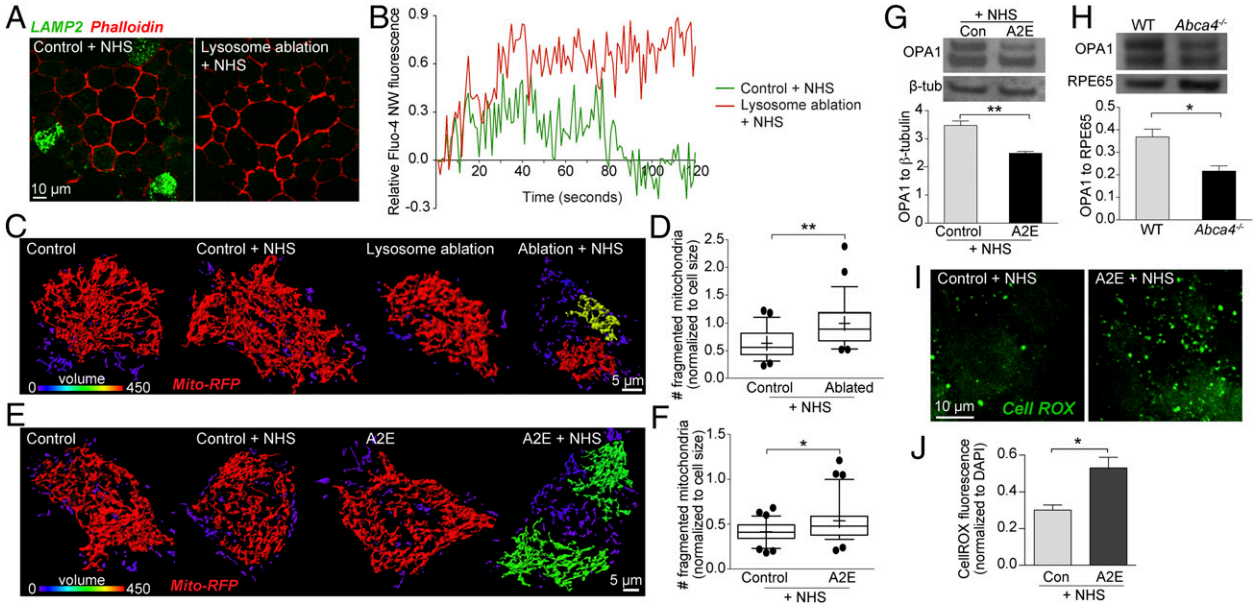

Fig. 4. Persistent sublytic MAC causes mitochondrial damage in the RPE. (*A*) Surface LAMP2 labeling (green) after exposure to 10% NHS in control cells and after lysosome ablation. Phalloidin (red) labels the actin cytoskeleton and demarcates cell boundaries. (*B*) Representative single-cell recording of intracellular calcium measured by Fluo-4 NW fluorescence in control (green curve) and lysosome-ablated (red curve) cells immediately after addition of 10% NHS. (*C*) Surface rendering of mitochondrial volume in RPE-expressing mito-RFP. Control and lysosome-ablated cells were exposed to 10% NHS. Color bar shows decreasing mitochondrial volume from red to violet (indicating increasing mitochondrial fragmentation). (*D*) Quantification of the number of mitochondrial fragments after NHS exposure. $^{**}P < 0.005$, 25 cells per condition. (*E*) Surface rendering of mitochondrial volume as in *C*. (*F*) Quantification of the number of mitochondrial fragments after NHS exposure. $^{*}P < 0.05$, $n \geq 31$ cells. (*G*) Representative immunoblot and quantification of OPA1 protein levels normalized to β-tubulin in primary polarized RPE after complement attack. Mean ± SEM, $n = 3$. $^{**}P < 0.005$. (*H*) Representative immunoblot and quantification of OPA1 protein levels normalized to RPE65 in RPE from wild-type and *Abca4*$^{-/-}$ mice. Mean ± SEM, $n = 3$. $^{*}P < 0.05$. (*I*) Stills from live imaging of CellROX labeling to monitor reactive oxygen species (green) in polarized primary RPE after exposure to 10% NHS for 10 min. (*J*) Quantitation of CellROX fluorescence. Mean ± SEM, $n = 3$ independent experiments. $^{*}P < 0.05$.

to elevated $[Ca^{2+}]_i$ (28). Analysis of the subcellular distribution of LAMP2-labeled lysosomes showed that there were significantly fewer lysosomes within 500 nm of the cell membrane in RPE with A2E (49.43 ± 1.8%) compared with control cells (58.43 ± 1.9%) (Fig. 3*F*). Taken together, these data demonstrate that sublytic complement attack stimulates lysosome exocytosis in the RPE. However, in cells with A2E, this is impaired because excess cholesterol and tubulin acetylation prevent MT-based transport of lysosomes to the cell periphery (31, 32).

Defective Lysosome Exocytosis Promotes Mitochondrial Damage After Complement Attack. To determine whether lysosome exocytosis is a critical response to sublytic MACs, we loaded RPE lysosomes with horseradish peroxidase (HRP) and ablated them with diaminobenzidine (DAB) (33). Inactivation of lysosomes was confirmed by loss of Lysosensor Blue labeling (Fig. S4*B*), whereas recycling endosomes labeled with Alexa-Transferrin were unaffected (Fig. S4*C*). Lysosome ablation prevented the appearance of LAMP2 on the RPE cell surface after exposure to NHS (Fig. 4*A*) or C9 (Fig. S4*D*). Live-cell imaging showed sustained elevation of $[Ca^{2+}]_i$ in lysosome-ablated RPE exposed to NHS compared with control cells whose $[Ca^{2+}]_i$ returned to baseline levels within 60 s (Fig. 4*B* and Fig. S4*E*).

Exposure to MACs over 12–24 h causes mitochondrial stress due to persistent increase in $[Ca^{2+}]_i$ (11, 24). Here, we asked whether defective lysosome exocytosis leads to mitochondrial damage in the RPE after a short exposure to complement. Live-cell imaging showed that the RPE mitochondrial network is remarkably robust with no appreciable fragmentation after exposure to 10% NHS for 10 min (Fig. 4*C*). However, in RPE with ablated lysosomes, complement attack increased mitochondrial fragmentation (Fig. 4 *C* and *D*). The mitochondrial network in RPE cells with A2E was similarly susceptible to fragmentation after two exposures to NHS over 48 h (Fig. 4 *E* and *F*), likely due to impaired lysosome exocytosis (Fig. 3 *A*–*E*).

To identify the mechanism underlying mitochondrial fragmentation, we measured the expression of optic atrophy 1 (OPA1), which mediates mitochondrial inner membrane fusion to maintain cristae architecture (34). Primary RPE with A2E (Fig. 4*G*) and RPE from *Abca4*$^{-/-}$ mice (Fig. 4*H*) had significantly less OPA1 protein compared with control RPE and RPE from wild-type mice, respectively. Mitochondrial fragmentation induced by sublytic MACs increased generation of reactive oxygen species (ROS) only in RPE with A2E, but not in control cells (Fig. 4*E*). These data provide strong support for the hypothesis that impaired CD59 recycling and lysosome exocytosis in RPE with vitamin A dimers make these cells vulnerable to complement-induced mitochondrial damage.

Strategies To Prevent Complement-Induced Injury in the RPE. In *Abca4*$^{-/-}$ RPE and primary RPE with A2E, excess cholesterol results in MT acetylation by activating ASMase (20). To establish that cholesterol-mediated activation of ASMase is responsible for impaired CD59 recycling and lysosome exocytosis, we treated polarized primary RPE monolayers with the liver X receptor alpha (LXRα) agonist TO901317 (TO; 1 μM, 16 h) to increase cholesterol efflux, or with the Food and Drug Administration-approved ASMase inhibitor desipramine (Des; 10 μM, 3 h) to decrease acetylated tubulin in RPE with A2E (20, 21). Both drugs restored surface CD59 (Fig. 5*A* and Fig. S4*A*) and lysosome exocytosis (Fig. 5*B* and Fig. S4*B*) in cells with A2E to levels seen in control RPE. Treatment with TO or Des also decreased ROS generation after complement exposure in RPE with A2E (Fig. S4*C*). Administration of TO to 5-mo-old *Abca4*$^{-/-}$ mice by intraperitoneal injections for 4 wk significantly decreased RPE cholesterol (Fig. 5*C*), restored CD59 to the apical surface of the RPE (Fig. 5*D*), and increased OPA1 expression (Fig. 5*E*).

Discussion

To maintain retinal homeostasis and limit inflammation in the face of aberrant complement activation, the RPE needs robust defense mechanisms that rapidly prevent MAC assembly and

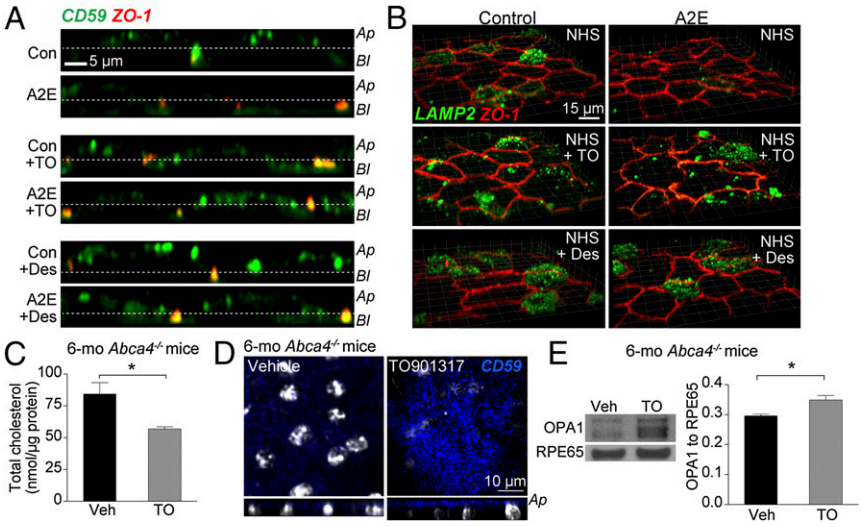

Fig. 5. Cholesterol removal or ASMase inhibition restores protective responses in the RPE. (*A*) Representative *x-z* scans of surface CD59 immunostaining (green) in polarized primary RPE cells (±A2E) untreated, or treated with either TO901317 (TO) or desipramine (Des). ZO-1 is in red. (*B*) Appearance of LAMP2 (green) on the plasma membrane after exposure to 10% NHS alone or after treatment with TO or Des. (*C*) Total cholesterol in the RPE of *Abca4*$^{-/-}$ mice administered either vehicle or TO (20 mg/kg, i.p.). Mean ± SEM, $n = 4$ animals per condition. *$P < 0.05$. (*D*) Single-plane *en face* and x-z confocal images of CD59 (blue) immunostaining in RPE flatmounts at the apical (Ap) surface in vehicle- or TO-treated *Abca4*$^{-/-}$ mice. (*E*) Representative immunoblot and quantification of OPA1 protein levels normalized to RPE65 in RPE from *Abca4*$^{-/-}$ mice administered either vehicle or TO. Mean ± SEM, $n = 4$ animals per condition. *$P < 0.05$.

eliminate MAC pores. Here, we identified two such responses occurring on timescales of seconds to minutes in the RPE—CD59 recycling and lysosome exocytosis—that are critical for countering sublytic MAC injury. Using pigmented *Abca4*$^{-/-}$ mice as a model for the early stages of Stargardt disease (35), our data also elucidate how vitamin A dimers compromise these rapid protective responses, resulting in RPE mitochondrial damage after sublytic MAC attack.

The membrane-bound complement regulator CD59 inhibits the final step of MAC formation, i.e., recruitment of C9 to the C5b-8 complex. Our data suggest that complement modulates CD59 trafficking to the RPE cell surface because exposure to C9 accelerated CD59 recycling. Nascent C5b-8 complexes cause conformational changes in CD59 necessary for it to bind C9 (15); therefore, increasing the amount of CD59 on the RPE plasma membrane could be a rapid way to combat assembly of functional MAC pores after complement attack. Live-cell imaging showed that complement exposure increased $[Ca^{2+}]_i$ and stimulated lysosome exocytosis. Lysosomal hydrolases and lipids released during exocytosis have been proposed to remodel the cell surface and limit membrane damage caused by pore-forming toxins (29). We show here that inactivating lysosomes causes sustained $[Ca^{2+}]_i$ elevation and mitochondrial fragmentation, indicating that lysosome exocytosis is a key mechanism for curtailing the downstream consequences of complement attack in the RPE.

Based on these data, we propose that the RPE has at least two distinct responses to sublytic MACs that differ primarily in the kinetics of their execution: CD59 recycling and lysosome exocytosis occur within minutes, as we have shown here. Endocytosis and lysosomal degradation of MACs by the RPE (11) and shedding of MACs into the extracellular medium (36) have been reported after tens of minutes or hours of exposure to complement; whether these mechanisms also occur over faster timescales remains to be determined. Data presented here and in other studies (11) show that defects in any of these mechanisms converge on a common pathway of mitochondrial damage in the RPE.

Despite increasing evidence that implicates the complement pathway in the etiology of Stargardt disease (7, 8) and AMD (3, 4), the mechanisms involved remain unclear. Our data show that in RPE with vitamin A dimers, cholesterol-induced MT acetylation (20) interfered with both CD59 recycling and lysosome exocytosis, leading to mitochondrial damage and oxidative stress after complement attack. Because oxidative stress affects mitochondrial fusion/fission dynamics, this could establish a self-propagating cycle of mitochondrial damage, inflammation, and dysfunction in the RPE. Finally, our experiments identify two therapeutic strategies to prevent complement-induced RPE damage: increasing cholesterol efflux by activating LXRα and decreasing MT acetylation by inhibiting ASMase (20). These data provide proof-of-concept validation of LXRα and ASMase as potential drug targets for Stargardt disease and other retinopathies associated with the accumulation of vitamin A dimers.

To date, approaches to target the complement pathway in macular degenerations have focused on complement proteins, with varying success (37). Our studies move beyond this narrow focus by providing insight into how the RPE deals with complement at a cellular level and by identifying drugs that can strengthen innate mechanisms essential for preserving RPE health.

Materials and Methods

Mice. Wild-type (Jackson Labs; 129S1/SvlmJ) and *Abca4*$^{-/-}$ mice (Jackson Labs; Abca4tm1Ght/J) were raised under 12-h cyclic light with standard diet. Mice were killed ~4–6 h after light onset, eyes were removed, and eyecups were processed for immunohistochemistry or immunoblotting (38). Studies were approved by the University of Wisconsin–Madison animal care and use authorities.

Primary Cell Culture. RPE were isolated from porcine retinas and plated at ~300,000 cells per square centimeter onto collagen-coated Transwell filters (Corning) to generate polarized RPE monolayers (20, 38).

Microscopy and Image Analysis. Imaging was performed on the Revolution XD dual spinning disk confocal/TIRF system (Andor). Images for a specific experiment were acquired using the same settings and analyzed using Imaris Spots and Surfaces modules (Bitplane) (20, 38).

Sublytic Complement Attack. Polarized RPE were exposed to either 10% NHS or 60 μg/mL purified C9 reconstituted in 10% C9-depleted serum (Quidel) for 10 min (11, 12). Heat-inactivated NHS (56 °C for 30 min) and C9-depleted sera were used as negative controls.

Treatments and Assays. Polarized RPE were treated with A2E (acute: 10 μM, 6 h followed by 48-h chase in fresh medium; chronic: 50 nM, 3 wk) (20). Other reagents used were LDL or OxLDL [both 50 μg/mL, 16 h (10); Athens Research & Technology], the ASMase inhibitor desipramine (10 μM, 3 h; Sigma) and the LXRα agonist TO901317 (1 μM, 16 h; Cayman) (20, 21). Cholesterol levels were measured with the Amplex Red cholesterol assay (ThermoFisher) (20).

Immunohistochemistry and Immunofluorescence. RPE flatmounts were fixed, incubated with primary antibodies [CD59 (1:50; LS Bio) and LAMP1 (1:100; Sigma)] overnight at 4 °C, followed by secondary antibodies for 2 h. Polarized primary porcine RPE were fixed, blocked with 1% BSA, and incubated with primary antibodies in 0.1% saponin (1 h) and secondary antibodies (30 min). For surface immunostaining, live cells were incubated with primary antibodies (30 min, 4 °C), fixed, permeabilized, and processed as above for ZO-1 labeling. Antibodies used were as follows: CD59 (1:100; ThermoFisher), LAMP2 (1:500; AbDSerotec), acetylated tubulin (1:1000; Sigma), C5b-9 (1:100; Novus), and ZO-1 (1:3000) (25). Other reagents were as follows: rhodamine-phalloidin (1:200, PHDR1; Cytoskeleton), Alexa-conjugated secondary antibodies (1:500), and DAPI (1:200), both from ThermoFisher.

Immunoblotting. RPE lysates were resolved using SDS/PAGE, proteins transferred to nitrocellulose membranes (ThermoFisher), and probed with rabbit anti-OPA1 (1:500; Novus), followed by HRP-conjugated secondary antibodies. β-Tubulin (1:500; Novus) and RPE65 (1:5000; Novus) were used as loading controls. Blots were visualized by ECL (ThermoFisher) and quantified with Image Studio (LI-COR).

CD59 Recycling. Cells were incubated with 1 U/mL PIPLC (ThermoFisher) for 1 h at 37 °C to cleave surface CD59, exposed to complement, and returned to normal growth medium (with 100 μg/mL cycloheximide to inhibit new protein synthesis) for indicated times. Cells were fixed, immunostained for surface CD59, and imaged as above.

TIRF Microscopy. RPE expressing pHluorin-Syt7 (30) were imaged at 37 °C immediately after addition of 10% NHS. TIRF angle was selected for the shallowest evanescent illumination, and images were captured every 10 s for 5 min.

Lysosome Exocytosis and Localization. RPE monolayers were exposed to complement, immediately transferred to ice and processed for surface LAMP2 staining. β-Hex activity in the media was measured as described previously (25) with 4-methyl-umbelliferyl-*N*-acetyl-β-D-glucosaminide (Sigma) as the substrate. For quantification of peripheral lysosomes, cells were transduced with CellLight Plasma Membrane-RFP (ThermoFisher), fixed, permeabilized, and stained for endogenous LAMP2. Cell surface and lysosomes were reconstructed in Imaris. Lysosomes within ≤500 nm from the plasma membrane were counted as peripheral lysosomes.

Lysosome Ablation. RPE cells were incubated with 5 mg/mL horseradish peroxidase (HRP; Sigma) in DMEM + 12 mM Hepes (1 h, 37 °C), rinsed, and incubated in fresh DMEM + 12 mM Hepes (2 h, 37 °C) to allow HRP uptake and transport to lysosomes (33). Cells were treated with 150 μg/mL DAB + 0.03% H_2O_2 in HBSS (1 h, 25 °C) to cross-link lysosomal proteins and ablate lysosomes. Control cells were similarly processed except for DAB treatment.

Calcium Imaging. Cells were loaded with Fluo-4 NW (ThermoFisher) for 30 min at 37 °C according to the manufacturer's protocol. Fields of interest were determined and imaging was initiated immediately after addition of 10% NHS. Images were captured at 37 °C at 1 frame per s for 2 min with 30 ms of exposure time. Mean intensity of Fluo-4 over time was calculated using Imaris.

Mitochondrial Dynamics and ROS. CellLight Mitochondria-RFP-expressing RPE were exposed to NHS and imaged live. Mitochondrial fragments were quantified and color-coded in Imaris. For ROS measurements, cells were incubated with 5 μM CellRox (37 °C, 30 min) and imaged live. CellROX fluorescence was measured at 640/665 excitation/emission (Ex/Em; Tecan) and normalized to DAPI fluorescence (Ex/Em: 360/460).

In Vivo Drug Treatments. *Abca4*$^{-/-}$ mice (males and females) were intraperitoneally injected three times a week for 4 wk with either 100 μL of 0.9% sodium chloride (Hospira) or 20 mg/kg T0901317 (Cayman) in 0.9% sodium chloride.

Statistics. Data were analyzed by using either a two-tailed *t* test or one-way ANOVA with the Bonferroni post hoc test (GraphPad Prism). Unless otherwise stated, data are presented as mean ± SEM of ≥3 independent experiments, with at least three to four replicates per condition per experiment.

ACKNOWLEDGMENTS. We thank Ed Chapman for the Syt7-pHluorin plasmid; Sara Amirahmadi for help with mouse work; and William Bement for helpful discussions. This work was supported by NIH Grants R01EY023299 and P30EY016665; BrightFocus Foundation Grant M2015350; Wisconsin Partnership Program New Investigator Program; Reeves Foundation; Macular Society UK; McPherson Eye Research Institute/Retina Research Foundation Rebecca Meyer Brown Professorship; Research to Prevent Blindness; and gifts from the Schuette-Kraemer family and the Christenson estate for macular degeneration research.

1. Perez VL, Caspi RR (2015) Immune mechanisms in inflammatory and degenerative eye disease. *Trends Immunol* 36(6):354–363.
2. McHarg S, Clark SJ, Day AJ, Bishop PN (2015) Age-related macular degeneration and the role of the complement system. *Mol Immunol* 67(1):43–50.
3. Sparrow JR, Ueda K, Zhou J (2012) Complement dysregulation in AMD: RPE-Bruch's membrane-choroid. *Mol Aspects Med* 33(4):436–445.
4. Bowes Rickman C, Farsiu S, Toth CA, Klingeborn M (2013) Dry age-related macular degeneration: Mechanisms, therapeutic targets, and imaging. *Invest Ophthalmol Vis Sci* 54(14):ORSF68–ORSF80.
5. Detrick B, Hooks JJ (2010) Immune regulation in the retina. *Immunol Res* 47(1-3):153–161.
6. Jiang M, et al. (2015) Microtubule motors transport phagosomes in the RPE, and lack of KLC1 leads to AMD-like pathogenesis. *J Cell Biol* 210(4):595–611.
7. Charbel Issa P, Barnard AR, Herrmann P, Washington I, MacLaren RE (2015) Rescue of the Stargardt phenotype in *Abca4* knockout mice through inhibition of vitamin A dimerization. *Proc Natl Acad Sci USA* 112(27):8415–8420.
8. Radu RA, et al. (2011) Complement system dysregulation and inflammation in the retinal pigment epithelium of a mouse model for Stargardt macular degeneration. *J Biol Chem* 286(21):18593–18601.
9. Zhou J, Jang YP, Kim SR, Sparrow JR (2006) Complement activation by photooxidation products of A2E, A lipofuscin constituent of the retinal pigment epithelium. *Proc Natl Acad Sci USA* 103(44):16182–16187.
10. Shaw PX, et al. (2012) Complement factor H genotypes impact risk of age-related macular degeneration by interaction with oxidized phospholipids. *Proc Natl Acad Sci USA* 109(34):13757–13762.
11. Georgiannakis A, et al. (2015) Retinal pigment epithelial cells mitigate the effects of complement attack by endocytosis of C5b-9. *J Immunol* 195(7):3382–3389.
12. Kunchithapautham K, Rohrer B (2011) Sublytic membrane-attack-complex (MAC) activation alters regulated rather than constitutive vascular endothelial growth factor (VEGF) secretion in retinal pigment epithelium monolayers. *J Biol Chem* 286(27):23717–23724.
13. Anderson DH, et al. (2010) The pivotal role of the complement system in aging and age-related macular degeneration: Hypothesis re-visited. *Prog Retin Eye Res* 29(2):95–112.
14. Lakkaraju A, Toops KA, Xu J (2014) Should I stay or should I go? Trafficking of sublytic MAC in the retinal pigment epithelium. *Adv Exp Med Biol* 801:267–274.
15. Bubeck D (2014) The making of a macromolecular machine: Assembly of the membrane attack complex. *Biochemistry* 53(12):1908–1915.
16. Ebrahimi KB, Fijalkowski N, Cano M, Handa JT (2013) Decreased membrane complement regulators in the retinal pigmented epithelium contributes to age-related macular degeneration. *J Pathol* 229(5):729–742.
17. Whitmore SS, et al. (2015) Complement activation and choriocapillaris loss in early AMD: Implications for pathophysiology and therapy. *Prog Retin Eye Res* 45:1–29.
18. Weismann D, et al. (2011) Complement factor H binds malondialdehyde epitopes and protects from oxidative stress. *Nature* 478(7367):76–81.
19. Sweigard JH, et al. (2015) Inhibition of the alternative complement pathway preserves photoreceptors after retinal injury. *Sci Transl Med* 7(297):297ra116.
20. Toops KA, Tan LX, Jiang Z, Radu RA, Lakkaraju A (2015) Cholesterol-mediated activation of acid sphingomyelinase disrupts autophagy in the retinal pigment epithelium. *Mol Biol Cell* 26(1):1–14.
21. Lakkaraju A, Finnemann SC, Rodriguez-Boulan E (2007) The lipofuscin fluorophore A2E perturbs cholesterol metabolism in retinal pigment epithelial cells. *Proc Natl Acad Sci USA* 104(26):11026–11031.
22. Mayor S, Riezman H (2004) Sorting GPI-anchored proteins. *Nat Rev Mol Cell Biol* 5(2):110–120.
23. Krus U, et al. (2014) The complement inhibitor CD59 regulates insulin secretion by modulating exocytotic events. *Cell Metab* 19(5):883–890.
24. Triantafilou K, Hughes TR, Triantafilou M, Morgan BP (2013) The complement membrane attack complex triggers intracellular Ca2+ fluxes leading to NLRP3 inflammasome activation. *J Cell Sci* 126(Pt 13):2903–2913.
25. Xu J, et al. (2012) Mechanism of polarized lysosome exocytosis in epithelial cells. *J Cell Sci* 125(Pt 24):5937–5943.
26. He Q, et al. (2014) Primary cilia in stem cells and neural progenitors are regulated by neutral sphingomyelinase 2 and ceramide. *Mol Biol Cell* 25(11):1715–1729.
27. Genewsky A, et al. (2015) Activation of endogenously expressed ion channels by active complement in the retinal pigment epithelium. *Pflugers Arch* 467(10):2179–2191.
28. Jaiswal JK, Andrews NW, Simon SM (2002) Membrane proximal lysosomes are the major vesicles responsible for calcium-dependent exocytosis in nonsecretory cells. *J Cell Biol* 159(4):625–635.
29. Andrews NW, Almeida PE, Corrotte M (2014) Damage control: Cellular mechanisms of plasma membrane repair. *Trends Cell Biol* 24(12):734–742.
30. Dean C, et al. (2012) Axonal and dendritic synaptotagmin isoforms revealed by a phluorin-syt functional screen. *Mol Biol Cell* 23(9):1715–1727.
31. Carta S, et al. (2006) Histone deacetylase inhibitors prevent exocytosis of interleukin-1beta-containing secretory lysosomes: Role of microtubules. *Blood* 108(5):1618–1626.
32. Rocha N, et al. (2009) Cholesterol sensor ORP1L contacts the ER protein VAP to control Rab7-RILP-p150 Glued and late endosome positioning. *J Cell Biol* 185(7):1209–1225.
33. Laulagnier K, et al. (2011) Role of AP1 and Gadkin in the traffic of secretory endolysosomes. *Mol Biol Cell* 22(12):2068–2082.
34. Olichon A, et al. (2003) Loss of OPA1 perturbates the mitochondrial inner membrane structure and integrity, leading to cytochrome c release and apoptosis. *J Biol Chem* 278(10):7743–7746.
35. Charbel Issa P, et al. (2013) Fundus autofluorescence in the Abca4(-/-) mouse model of Stargardt disease—Correlation with accumulation of A2E, retinal function, and histology. *Invest Ophthalmol Vis Sci* 54(8):5602–5612.
36. Thurman JM, et al. (2009) Oxidative stress renders retinal pigment epithelial cells susceptible to complement-mediated injury. *J Biol Chem* 284(25):16939–16947.
37. Holz FG, Schmitz-Valckenberg S, Fleckenstein M (2014) Recent developments in the treatment of age-related macular degeneration. *J Clin Invest* 124(4):1430–1438.
38. Toops KA, Tan LX, Lakkaraju A (2014) A detailed three-step protocol for live imaging of intracellular traffic in polarized primary porcine RPE monolayers. *Exp Eye Res* 124:74–85.

Supporting Information

Tan et al. 10.1073/pnas.1523061113

SI Materials and Methods

Mice. Wild-type (Jackson Labs; 129S1/SvlmJ, stock no. 002448) and *Abca4*$^{-/-}$ mice (Jackson Labs; Abca4tm1Ght/J, stock no. 023725) were raised under 12-h cyclic light and fed a standard rodent diet (NIH-31, 7013; Harlan Teklad). Mice were killed ∼4–6 h after light onset, and eyes were removed and hemisected. The anterior portion containing the cornea, lens, and vitreous was discarded. Eyecups were processed for immunohistochemistry or immunoblotting (20). All studies were approved by the University of Wisconsin–Madison animal care and use authorities.

Primary RPE Cell Culture. RPE were isolated from porcine retinas as described previously (20, 38). Cells were plated at confluence (∼300,000 cells per square centimeter) onto collagen-coated Transwell filters (Corning). After 2 wk, cells formed highly pigmented polarized monolayers with transepithelial electrical resistances of >300 ohm/cm^2.

Microscopy and Image Analysis. All imaging was performed on the Revolution XD (RevXD) system (Andor) equipped with: an inverted Eclipse Ti microscope base with TIRF arm (Nikon), CSU-X1 confocal spinning disk head (Yokagawa), iXon3 897 EM-CCD camera (Andor; for confocal), Neo sCMOS camera (Andor; for TIRF), 60× Plan Apo VC objective (Nikon; N.A. 1.4), 100× Apo TIRF objective (Nikon; N.A. 1.49), 1.5× Optivar optical zoom (Nikon), CO_2 cage incubator and environmental chamber (Okolab), four color laser combiner (Andor), and IQ3 imaging software (Andor) as described in detail previously (20, 38). All images collected during a specific experiment were acquired using the same objective, exposure, laser excitation, and gain parameters. Images were analyzed using Imaris software v 7.6.1 (Bitplane) equipped with Spots and Surfaces modules. In Imaris, images collected during a specific experiment were subjected to the same background subtraction and Gaussian smoothing algorithms where appropriate as described in refs. 20 and 38.

Sublytic Complement Attack. RPE on Transwell filters were exposed to either 10% NHS or 60 μg/mL purified C9 reconstituted in 10% C9-depleted serum (all from Quidel) for 10 min to induce sublytic MAC deposition (11, 12). Heat-inactivated NHS (56 °C for 30 min) and C9-depleted sera were used as negative controls. Porcine RPE are sensitive to human complement components (11), and human serum has been reported to contain 10–20 times C9 molecules in excess of that required for sublytic MACs (12). To confirm that the effects seen with NHS are due to C5b-9 assembly, we used 60 μg/mL purified C9 (Quidel) reconstituted with 10% C9-depleted serum (Quidel) to induce complement attack. Note that 60 μg/mL is the concentration present in 100% serum (11). Cytotoxicity after NHS or C9 treatments was monitored by using the lactate dehydrogenase assay (LDH assay kit; ThermoFisher) according to the manufacturer's protocol. Background values due to presence of serum were deducted from the experimental values for each condition.

Pharmacological Treatments and Assays. The lipofuscin bisretinoid A2E was synthesized and purified as described previously (>97%, ESI-MS) (21). RPE were exposed to either a chronic low-dose of A2E (50 nM for 3 wk) or an acute high-dose of A2E (10 μM for 6 h, followed by a 48-h chase in fresh culture medium). Our published data show that these treatments result in intracellular A2E levels similar to those found in the RPE of patients with Stargardt disease and in the *Abca4*$^{-/-}$ mice (20). Other drugs used were LDL or OxLDL [50 μg/mL for 16 h (10); Athens Research & Technology], U18666A (2.5 μM for 16 h), the HDAC6 inhibitor tubacin (2 μM for 16 h), the ASMase inhibitor desipramine (10 μM for 3 h), all from Sigma, and the LXRα agonist TO901317 (1 μM for 16 h; Cayman Chemicals) (20, 21). Cholesterol levels were measured from RPE lysates by using the Amplex Red cholesterol assay kit (ThermoFisher) (20, 21).

Immunohistochemistry. For RPE flatmounts, the anterior segment and lens were removed and four deep relaxing cuts were made to the eyecup. Eyecups were fixed in 3.7% (vol/vol) paraformaldehyde (PFA) in PBS for 2 h at room temperature and washed in PBS. The retina was removed and four additional cuts were made. The resulting RPE flatmounts were blocked in 2% (vol/vol) BSA with 0.1% Triton X-100 in PBS for 1 h at room temperature. Flatmounts were incubated with the following primary antibodies: mouse anti-CD59 (1:50; LS Bio, LS-C210252), rabbit anti-LAMP1 (1:100; Sigma, L1418), rabbit anti-α-catenin (1:1000; Sigma, C2081) in 1% BSA in PBS overnight at 4 °C. Flatmounts were washed and incubated with Alexa-conjugated secondary antibodies (1:500; ThermoFisher) in 1% BSA in PBS for 2 h at room temperature protected from light. After DAPI labeling and mounting on slides, flatmounts were imaged with the Andor Revolution system, 60× objective 1.4 N.A. oil objective with identical exposures and gains and 1.5× Optivar optical zoom.

Cryosections of wild-type and *Abca4*$^{-/-}$ mice retinas were blocked in PBS with 4% (vol/vol) BSA and incubated with 1:50 mouse anti-CD59 (LS Bio, LS-C210252) or 1:50 mouse IgG control (Thermo Scientific; 02–6502) for 48 h at 4 °C in a humidified chamber. Slides were rinsed to remove unbound antibodies and incubated with Alexa-conjugated secondary antibody [1:500 in PBS with 4% (vol/vol) BSA] for 18 h at 4 °C in a humidified chamber protected from light. Sections were rinsed, stained with DAPI, rinsed, and sealed under coverslips by using Vectashield (Vector Labs) as a mounting medium. Slides were imaged with the Andor Revolution XD spinning disk confocal microscope by using a 60× 1.4 N.A. oil objective with identical exposures and gains.

Immunoblotting. RPE were lysed in HNTG buffer [50 mM Hepes, 150 mM NaCl, 10% (vol/vol) glycerol, 1.5 mM $MgCl_2$, 1% TX-100] with protease inhibitors (Calbiochem). Equal amounts of protein (20 μg) were resolved in 4–12% NuPAGE Bis-Tris Gels and transferred onto nitrocellulose membranes (ThermoFisher). Membranes were probed with mouse anti-CD59 [for porcine RPE: 1:500 clone MEM43 (ThermoFisher MA1-19133); for mouse RPE: 1:200 (LSBio, LS-C210252)] and rabbit anti-OPA1 (1:500; NB110-55290; Novus), followed by HRP-conjugated secondary antibodies. Rabbit anti–β-tubulin (1:500; Novus NB600-936) and mouse anti-RPE65 (1:5000; Novus NB100-355) were used as loading controls for porcine and mouse samples, respectively. Blots were visualized by ECL (ThermoFisher) and quantified with Image Studio (LI-COR).

Analysis of Cell Surface CD59. RPE monolayers were fixed in 2% (vol/vol) PFA (Electron Microscopy Sciences), blocked in 1% BSA in PBS and incubated with mouse anti-CD59 (1:100; clone MEM-43, ThermoFisher MA1-19133) for 1 h at 25 °C. This antibody recognizes the extracellular epitope of CD59 and labels CD59 on the plasma membrane in nonpermeabilized cells. After removing unbound antibody, cells were briefly fixed [2% (vol/vol) PFA, 5 min], rinsed, and permeabilized with 0.1% saponin in PBS with 1% BSA.

Cells were stained with rat anti–ZO-1 (1:3,000) (25). Cells were imaged on the Andor Revolution XD spinning disk confocal microscope by using a 100× 1.49 N.A. oil objective with identical exposures and gains. Fluorescence intensity of CD59 was quantified by using the Surface module in Imaris (Bitplane).

Analysis of MAC Deposition. Cells were incubated live with mouse anti-C5b-9 (1:100; clone aE11, Novus NBP1-05120) at 4 °C for 30 min, fixed, permeabilized, stained for ZO-1, and imaged as above. MAC puncta per cell were quantified using Imaris (Bitplane).

Analysis of CD59 Recycling. To measure CD59 recycling, cells were incubated with 1 U/mL PI-PLC (ThermoFisher) for 1 h at 37 °C to cleave surface CD59 and exposed to either 10% NHS or 60 μg/mL C9 in C9-depleted serum for 10 min. Cells were returned to normal growth medium (with 100 μg/mL cycloheximide to inhibit new protein synthesis) for indicated times. Cells were fixed, immunostained for surface CD59, and imaged as above. In the thresholding criteria step of the Surface module of Imaris used to quantify surface CD59 fluorescence, we defined a minimum number of voxels for the signal-to-noise ratio and a minimum fluorescence signal intensity. These criteria were held constant within a set of experiments. Data are presented as relative CD59 fluorescence normalized to cell number for each treatment condition and do not represent the absolute amount of CD59 on the cell surface. We also analyzed the signal from the "no primary antibody" controls, which is mainly low-level autofluorescence that can be clearly distinguished from the CD59 antibody-stained samples.

Immunofluorescence. Primary RPE monolayers on Transwell filters were fixed in 2% (vol/vol) PFA, blocked in PBS with 1% BSA for 30 min at room temperature, and stained with mouse anti-acetylated-tubulin (1:1000; clone 6-11B-1, Sigma T6793) and rat anti–ZO-1 (1:3,000) (25) in the presence of 0.1% saponin for 1 h. After removal of unbound antibodies, cells were incubated in AlexaFluor secondary antibodies (1:500 in PBS with 1% BSA) for 30 min at room temperature in the dark. DAPI (1:200; ThermoFisher) was used to stain cell nuclei. Where applicable, rhodamine-phalloidin (1:200; Cytoskeleton, PHDR1) was added along with the secondary antibodies to label the actin cytoskeleton.

Live Imaging of Lysosome Exocytosis Using TIRF Microscopy. Primary RPE (~1.5×10^6) were nucleofected (Amaxa; Lonza) with 10 μg of pHluorin-tagged synaptotagmin-VII (30). Transfection efficiencies were ≥40%. Cells were transferred to the microscope stage enclosed in a humidified chamber (Okolab) and imaged at 37 °C on the Andor system [100× 1.49 N.A. Apo TIRF objective (Nikon), Neo sCMOS camera (Andor)] after addition of 10% NHS. The TIRF angle was selected for the shallowest evanescent illumination (28), and images were captured every 10 s for 5 min. Exocytic events were quantified with the Spots module with threshold parameters determined manually to account for cell-to-cell variability in pHluorin expression.

Detection of Cell Surface LAMP2. RPE monolayers were exposed to 10% NHS or 60 μg/mL C9 in C9-depleted serum for 10 min, immediately transferred to ice, and incubated at 4 °C for 30 min with mouse anti-LAMP2 (1:500, clone AC17, MCA2558; ABDSerotec), which recognizes the luminal domain of LAMP2. Cells were fixed, permeabilized and stained for rat anti-ZO-1 (1:3,000) (25). Surface LAMP2 levels were quantified from confocal images by using Imaris.

β-Hex Activity. The β-Hex assay was performed as detailed previously (25). Briefly, apical and basolateral media were collected, centrifuged to pellet dead cells and debris. Supernatant (350 μL) was incubated with 50 μL of 6 mM 4-methyl-umbelliferyl-*N*-acetyl-β-D-glucosaminide (Sigma) in sodium citrate-phosphate buffer, pH 4.5, and fluorescence was measured at 365 nm (450 nm emission) on a microplate reader (Tecan). Cell lysates (5 μL) were used to measure total cellular β-hex activity.

Analysis of Lysosome Localization. For quantification of peripheral lysosomes, cells were transduced with BacMAM CellLight Plasma Membrane-RFP (ThermoFisher). Cells were incubated with 15 viral particles per cell overnight. Transduction efficiency was ≥60%. Cells were fixed, permeabilized, and stained with mouse anti-LAMP2 (1:500; clone AC17, AbDSerotec MCA2558) as above. Cell surfaces and lysosomes were then reconstructed by using the Surface and Spots modules in Imaris, respectively. Lysosomes within 0.5 μm from the plasma membrane were counted as peripheral lysosomes.

Lysosome Ablation. This protocol was adapted from published reports (33). Briefly, cells were incubated with 5 mg/mL horseradish peroxidase (HRP; Sigma) in DMEM with 12 mM Hepes for 1 h at 37 °C to allow internalization of HRP. Uninternalized HRP was removed by rinsing five times with 5% (vol/vol) BSA in PBS with Ca^{2+} and Mg^{2+}. Cells were then incubated in DMEM with 12 mM Hepes for 2 h at 37 °C to allow HRP to traffic to lysosomes. Cells were rinsed five times as above, and lysosomal proteins were cross-linked with 150 μg/mL DAB and 0.03% H_2O_2 in HBSS for 1 h at room temperature. Excess DAB was removed by rinsing with HBSS. To confirm that lysosomes were inactivated by ablation, cells were incubated with Lysosensor blue (7.5 μL/mL; Thermo Fisher L7533) and CellMask orange (0.5 μl/mL; Thermo Fisher C10045) for 5 min at 37 °C in the dark. Cells were rinsed to remove excess dyes and imaged immediately on the Andor Revolution XD microscope with the 100× 1.49 N.A. oil objective. In parallel experiments, Alexa488-Transferrin (50 μg/mL, 15 min at 37 °C; Thermo Fisher T13342) was used to label recycling endosomes and imaged as above.

Calcium Imaging. Cells were loaded with Fluo-4 NW (F36206; Thermo Scientific) for 30 min at 37 °C according to the manufacturer's protocol. Fields of interest were determined, and imaging was initiated immediately after addition of 10% NHS. Images were captured at 37 °C on the Andor system [100× 1.49 N.A. objective (Nikon), iXon x3 897 EM-CCD camera] at 1 frame per s for 2 min with 30 ms of exposure time. Mean intensity of Fluo-4 dye over time was obtained with Imaris (Bitplane).

Live Imaging of Mitochondrial Dynamics. RPE were transduced with ~15 particles per cell of BacMAM CellLight Mitochondria-RFP. Transduction efficiency was ≥60%. Cells were exposed to 10% NHS and imaged live because the tubular mitochondrial network is not preserved after fixation. The number and volume of mitochondrial fragments were quantified by 3D surface rendering (Imaris). The Surface module takes a 3D dataset, as from confocal imaging, and uses an object identification algorithm with user-defined threshold criteria to build artificial solid objects within the image that can be measured for statistics such as the number of discrete or connected objects and the object's volumes. Automated segmentation of these objects by color-coding, based on volume of the connected components, was used for 3D surface rendering of these objects. Data in Fig. 4 are presented as maximum intensity projections of the object data set using the Surpass mode of Imaris.

Quantification of ROS. After complement attack, cells were rinsed, incubated with 5 μM CellROX (37 °C, 30 min), and imaged live (Andor RevXD). For quantification, CellROX fluorescence was measured with a microplate reader (Tecan) at Ex/Em of 640/665 and normalized to DAPI fluorescence (Ex/Em: 360/460).

In Vivo Drug Treatments. Four-month-old *Abca4*$^{-/-}$ mice (males and females) were intraperitoneally injected three times a week for 4 wk

with either 100 μL of 10% (vol/vol) DMSO in 0.9% sodium chloride (Hospira) or 20 mg/kg T0901317 (Cayman Chemicals) in 10% (vol/vol) DMSO in 0.9% sodium chloride. After completion of treatment regimens, animals were killed and RPE processed for cholesterol measurements, immunostaining, or immunoblotting as detailed above.

Statistics. Data were analyzed by using either a two-tailed *t* test or one-way ANOVA with the Bonferroni post hoc test (GraphPad Prism). Unless otherwise stated, data are presented as mean ± SEM of ≥3 independent experiments, with at least three to four replicates per condition per experiment.

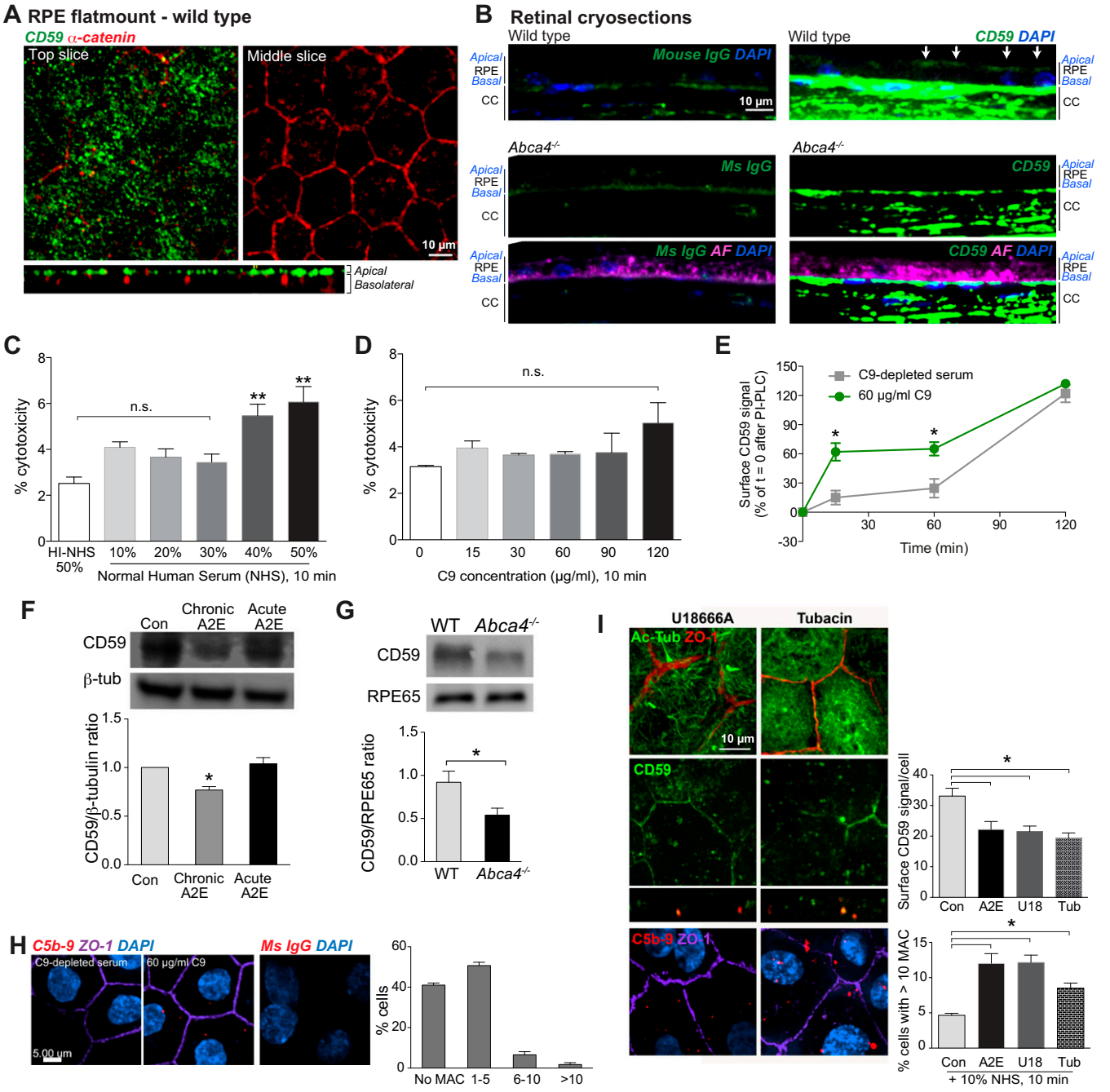

Fig. S1. (*A*) Single-plane *en face* and *x-z* confocal images of CD59 immunofluorescence (green) in flatmounts of mouse RPE. Top (at the apical surface) and middle (through the center of the cell) slices are shown. α-Catenin (red) was used to label the basolateral membrane of the RPE. (*B*) Immunostaining (green) of wild-type and *Abca4*$^{-/-}$ retinal cryosections. Left images show nonspecific signal with mouse IgG. Images on the right show CD59 immunofluorescence (green) using a mouse monoclonal antibody. White arrows: apical surface of the RPE. AF, lipofuscin autofluorescence (pink); CC, choriocapillaris; nuclear marker DAPI (blue). (*C* and *D*) Cytotoxicity as a function of lactate dehydrogenase release after exposure to increasing concentrations of NHS (*C*) or purified C9 in 10% C9-depleted serum (*D*). Mean ± SEM, $n = 3$. $^{**}P < 0.001$ relative to 50% heat-inactivated NHS. n.s., not significant. (*E*) Recovery of CD59 fluorescence at the cell surface after PI-PLC treatment in RPE exposed to 10% C9-depleted serum (gray squares) or to 60 μg/mL C9 in C9-depleted serum for 10 min (green circles). Experiments were performed in the presence of cycloheximide to prevent new protein synthesis. For each condition, values are normalized to surface CD59 levels at $t = 0$ after PI-PLC treatment. Mean ± SEM, $n \geq 240$ cells per condition. $^{*}P < 0.05$. (*F*) Representative immunoblot and quantification of CD59 protein levels in primary porcine RPE monolayers treated or not with A2E. Chronic: 50 nM A2E for 3 wk; acute: 10 μM A2E for 6 h followed by a 48-h chase (20). Mean ± SEM, $n = 3$. $^{*}P < 0.05$. (*G*) Representative immunoblot and quantification of CD59 protein levels in RPE from wild-type and *Abca4*$^{-/-}$ mice. RPE65 is the loading control. Mean ± SEM, $n = 3$. $^{*}P < 0.05$. (*H*) Images of MACs (red) on the RPE surface after exposure to 10% C9-depleted serum or 60 μg/mL C9 in 10% C9-depleted serum for 10 min. ZO-1 is in purple, and DAPI is in blue. Graph shows quantification of MAC deposition on cells exposed to 60 μg/mL C9 in C9-depleted serum. A total of 206 cells were analyzed. The image on the *Right* shows mouse IgG staining as a negative control. (*I*) Immunofluorescence images of acetylated tubulin (green, *Top*), CD59 (green, *Middle*), and C5b-9 (red, *Bottom*) in primary RPE treated with 2.5 μM U18666A or 500 nM tubacin for 16 h. For CD59 quantification, Mean ± SEM of ≥ 180 cells per condition. $^{*}P < 0.01$. For MAC quantification, cells with ≥10 MACs per cell are presented as mean ± SEM, $n \geq 150$ cells per condition. $^{*}P < 0.005$ relative to control cells exposed to NHS.

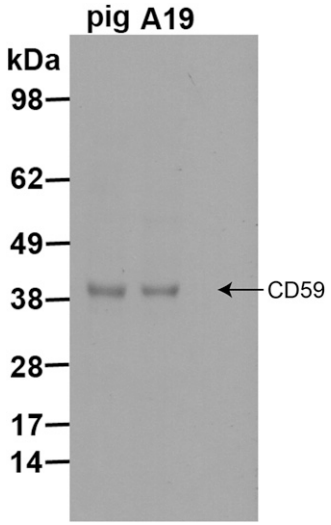

Fig. S2. Validation of the CD59 antibody (clone MEM43) in porcine RPE. Representative immunoblot comparing primary porcine RPE and human ARPE-19 cell lysates is shown. The MEM43 clone recognizes an epitope in CD59 (specific residues W40, L53) that is conserved in both pig and humans.

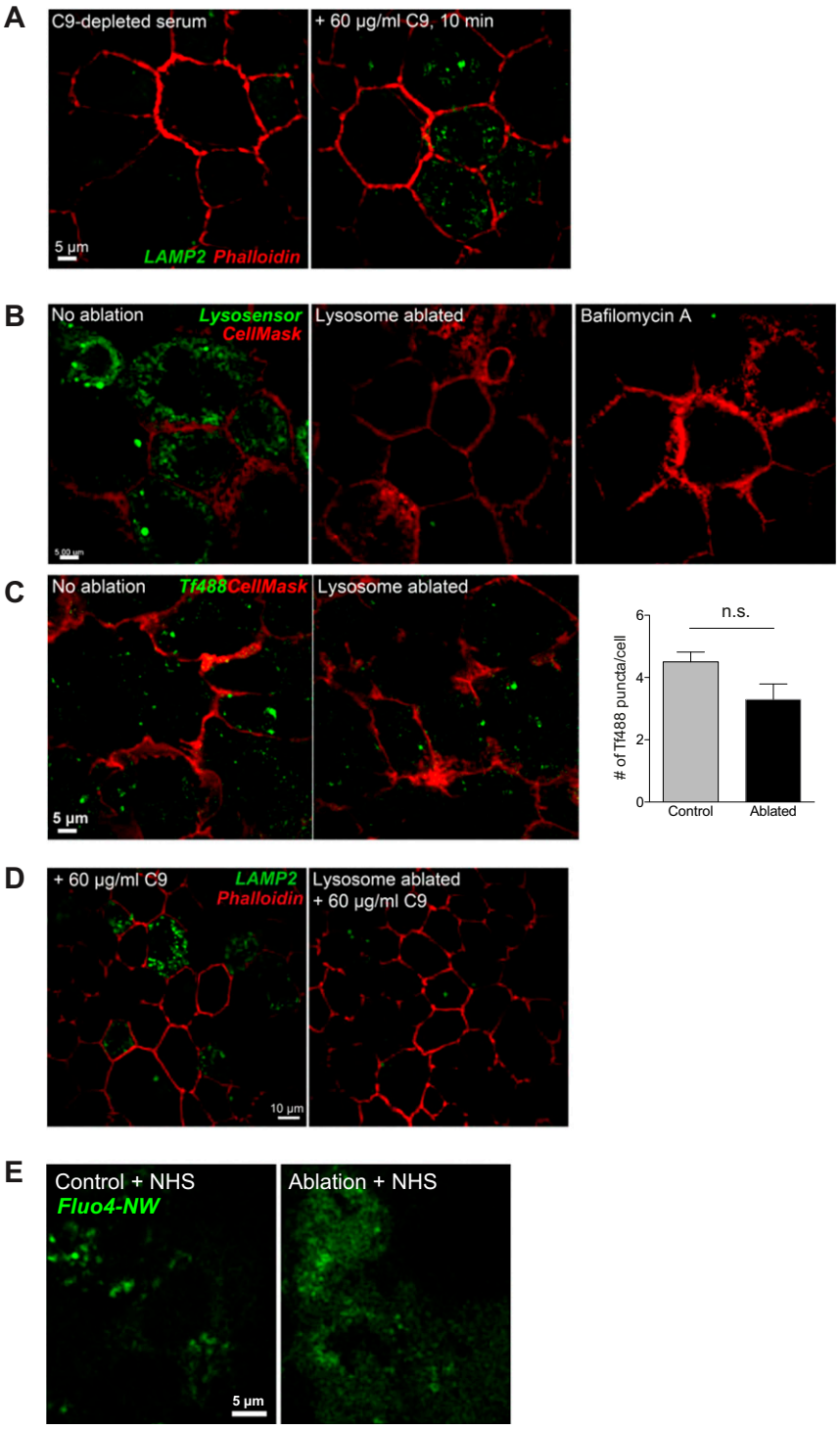

Fig. S3. (*A*) Immunofluorescence images of surface LAMP2 labeling (green) on the surface of live cells after exposure to either 10% C9-depleted serum or 60 µg/mL C9 in 10% C9-depleted serum for 10 min. Phalloidin is in red. (*B*) Stills from live imaging of Lysosensor (green) labeling of lysosomes in control RPE monolayers or after lysosome ablation. The vacuolar ATPase inhibitor bafilomycin A1 was used as a positive control. (*C*) Stills from live imaging and quantitation of recycling endosomes labeled with Alexa488-Transferrin (green) in control RPE or after lysosome ablation; n.s., not significant. In *B* and *C*, CellMask (red) was used to label the plasma membrane. (*D*) Immunofluorescence images of surface LAMP2 labeling (green) after exposure to 60 µg/mL C9 in control cells and after lysosome ablation. Phalloidin (red) was used to demarcate cell boundaries. (*E*) Stills from live imaging of Fluo-4 NW to measure calcium influx in control and lysosome-ablated cells after addition of 10% NHS.

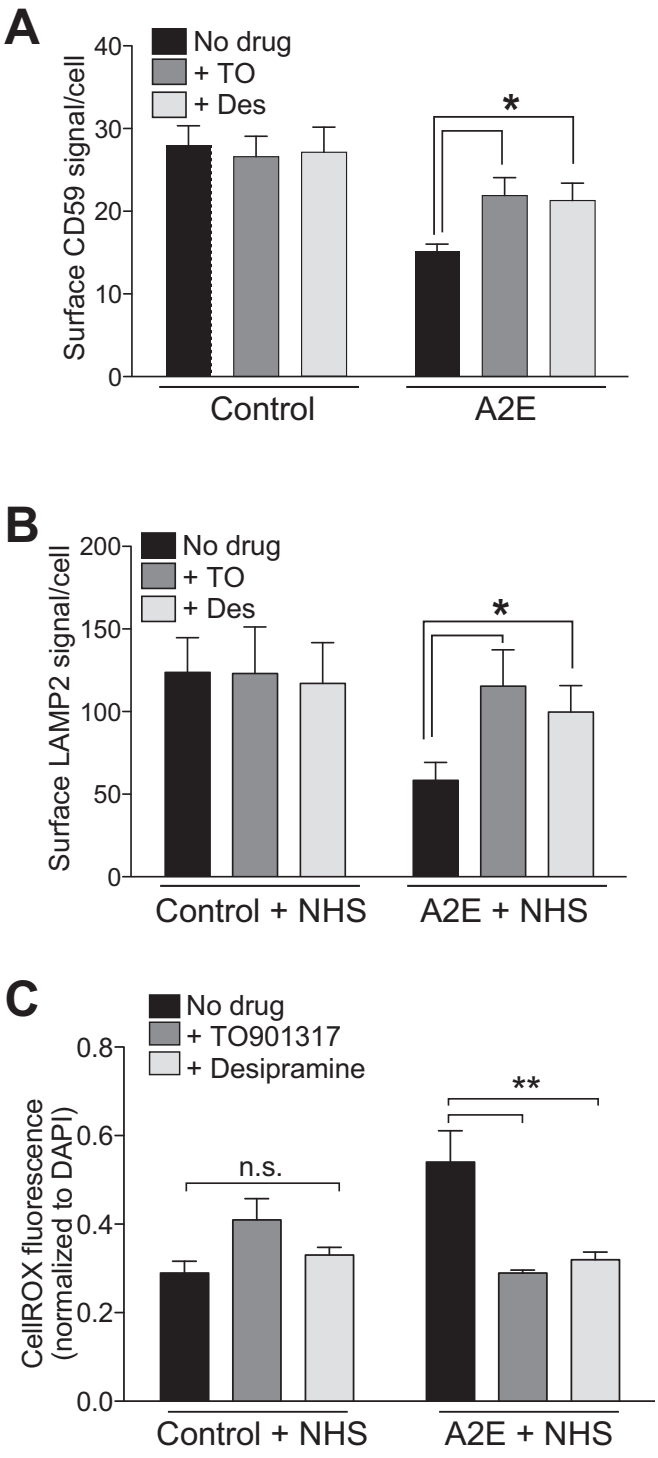

Fig. S4. (*A*) Quantification of surface CD59 immunostaining in polarized primary RPE cells, untreated or treated with either the LXR agonist TO901317 (TO) or the ASMase inhibitor desipramine (Des). Mean fluorescence ± SEM, $n = 100$ cells per condition. *$P < 0.05$. (*B*) Quantification of surface LAMP2 fluorescence after exposure to 10% NHS alone or after treatment with TO or Des. Mean ± SEM, $n = 150$ cells per condition. *$P < 0.05$. (*C*) Quantification of ROS using CellRox before and after exposure to NHS ± TO or Des. Mean ± SEM, $n = 3$. **$P < 0.005$, one-way ANOVA with Bonferroni's post hoc test.

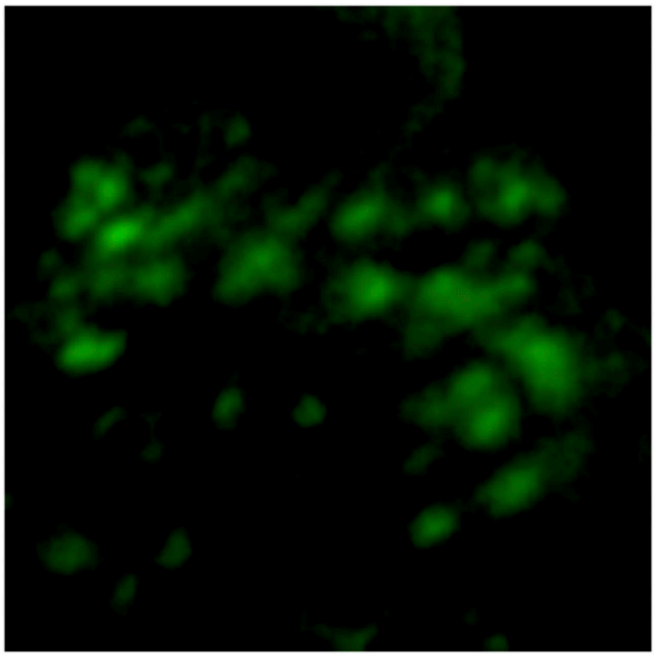

Movie S1. Primary RPE cells transfected with Syt7-pHluorin were imaged by TIRF microscopy at 37 °C (Andor Revolution XD system). Cells were exposed to 10% NHS immediately before imaging and images were acquired continuously for 5 min.

Movie S1

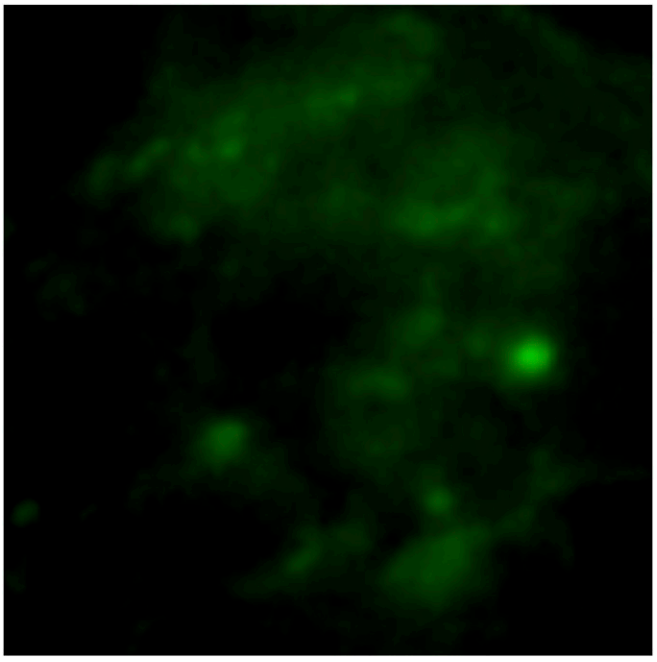

Movie S2. Primary RPE cells were transfected with Syt7-pHluorin and treated with A2E (10 μM, 6 h, followed by 48-h chase in fresh medium) (20, 21). Cells were imaged by TIRF microscopy at 37 °C (Andor Revolution XD system). Cells were exposed to 10% NHS immediately before imaging and images were acquired continuously for 5 min.

Movie S2